搅拌摩擦焊接过程中材料流动形式

张 昭, 刘亚丽, 陈金涛, 张洪武
(大连理工大学 工业装备结构分析国家重点实验室, 辽宁 大连 116024)

摘 要: 采用完全热力耦合模型对搅拌摩擦焊接过程进行模拟, 并详细分析了搅拌摩擦焊接过程中的材料流动形式。结果表明, 模型可以成功预测搅拌摩擦焊接过程材料流动和温度分布情况。通过对搅拌头周围材料流动的研究, 分析了搅拌摩擦焊接过程中飞边现象形成的主要原因。研究了搅拌摩擦焊接构件不同厚度上材料的三维流动形式, 通过与二维情况的比较证实, 二维情况下的材料流动数值模拟结果对应于搅拌摩擦焊接构件靠近下表面部分的材料流动情况。从等效塑性应变的分布也能证实搅拌头轴肩对靠近上表面的材料行为具有明显影响, 而对下表面附近材料行为影响较弱, 从而说明二维情况对应三维情况靠近下表面的部分。

关键词: 搅拌摩擦焊接; 完全热力耦合模型; 材料流动; 有限元法
中图分类号: TG402; TG404 文献标识码: A 文章编号: 0253-360X(2007)11-017-05

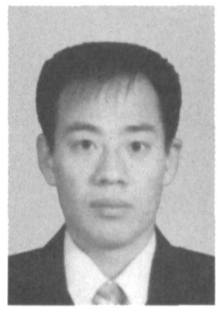

张 昭

0 序 言

搅拌摩擦焊接技术是一种新型焊接工艺, 具有节能、环保和适应性广等特点, 自发明以来, 迅速应用到航空航天、船舶以及汽车制造等工业领域。搅拌摩擦焊接的基本原理是将一个旋转的搅拌头插入对接的焊缝中, 通过搅拌头的不停旋转以及沿焊缝方向的平移使焊缝两侧的金属充分搅拌, 从而实现可靠连接。

搅拌摩擦焊接涉及热力耦合、大变形、材料显微结构和性质的变化等, 是一个复杂的过程, 因此, 搅拌摩擦焊接发明以来, 吸引了众多学者的注意并开展了多项研究。王大勇等人[1] 对 Al-Li 合金搅拌摩擦焊接头的研究发现搅拌摩擦焊接头发生软化并且前进侧软化区大于后退侧。Liu 等人[2] 认为 Al-Cu 合金的搅拌摩擦焊接"之行线"的出现会对热处理后的焊接构件的力学性能产生明显影响。Feng 等人[3] 的工作表明焊后热处理会导致焊接构件搅拌区材料晶粒粗化, 粗化程度与溶解温度有关。Reynolds 等人[4] 则研究了焊接参数的变化对 7050 铝合金搅拌摩擦焊接构件温度以及硬度分布的影响。

基于搅拌摩擦焊接技术的基本原理, Mishra 等人[5] 提出了搅拌摩擦加工技术, 用于生产具有高应变率超塑性的材料。Ma 等人[6] 对这一问题进行更为细致的研究, 通过研究发现搅拌摩擦加工技术可以使显微结构细化并且变得更为均匀, 这对于提高材料的性能是非常重要的。

由于搅拌摩擦焊接过程中, 焊接构件靠近上表面的材料不仅受到搅拌针的搅拌作用, 同时还要受到轴肩的旋转作用, 因此, 靠近上表面的材料具有和下表面材料不同的变形[7], 从而推知焊接构件上下表面材料应该具有不同的流动行为。目前还没有相关的工作来较为直观地显示和跟踪材料质点在搅拌摩擦焊接过程中的三维运动行为, 尽管文献[8] 跟踪了搅拌摩擦焊接过程中材料物质点的二维流动情况, 并取得了和试验一致的结果, 但是二维模型不能反映三维情况, 因此, 基于文献[8] 的工作, 进一步完善了搅拌摩擦焊接的数值模型, 采用有限元方法模拟搅拌摩擦焊接的完全热力耦合过程, 并着重分析搅拌摩擦焊接过程中的材料质点的三维迁移形式, 并对比不同厚度上材料流动形式的差异。

1 有限元模型

1.1 几何模型及边界条件

焊具采用刚体, 具体尺寸如图 1 所示, 共划分 1 877个四节点刚体单元, 包含 1 879 个节点。值得

收稿日期: 2007-01-25
基金项目: 国家自然科学基金资助项目(10225212, 10421202, 10302007); 国家基础性研究发展规划资助项目(2005CB321704); 长江学者和创新团队发展计划资助项目

注意的是，模型的轴肩有一个内凹角，大小为 80.5°。搅拌针的长度约为 8 mm，大于焊接构件的板厚(3 mm)，与实际加工情况稍有不同，主要是因为如果搅拌针的长度小于焊接构件厚度，将会导致求解奇异。由于在具体的计算求解中，焊接构件的下表面固定，因此，搅拌针的长度只要大于焊接构件的板厚就可以保证计算的顺利进行，此时，搅拌针的具体长度则不会明显影响求解的结果。在轴肩上方施加一个轴向载荷以阻止搅拌头下方材料的可能涌起，保证搅拌摩擦焊接过程顺利完成。为了方便计算，搅拌头倾角取为 0°。

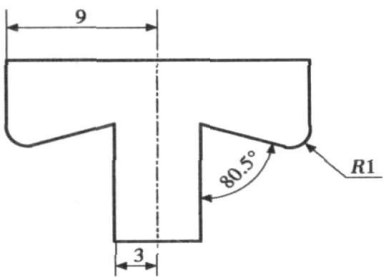

图 1 焊具尺寸(mm)

Fig. 1 Size of welding tool

搅拌头插入焊接构件的交接处，首先进行绕自身轴线的旋转，旋转速度为 400 r/min，这个过程持续 2 s。

焊接构件的材料为 Al6061—T6 合金，材料性质与温度相关[8]，焊接构件的具体尺寸如图 2 所示。焊接构件共划分 10 500 个六面体单元和 12 480 个节点，节点的自由度包含三个方向的移动和温度。为了方便计算，平移速度为 2 mm/s，模拟焊接得到的焊缝长度为 24 mm，平移速度被施加到焊接结构上，以等效于焊具向相反方向移动。

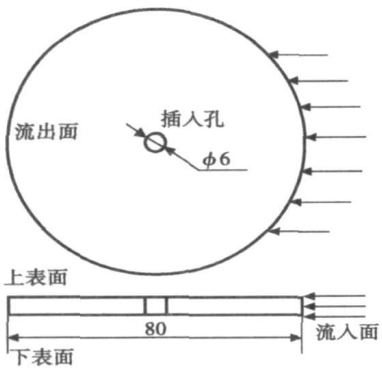

图 2 焊接构件尺寸及边界条件(mm)

Fig. 2 Boundaries and size of welding plate

1.2 接触定义

在搅拌摩擦焊接过程中的热量主要是由于搅拌头与工件的摩擦产生。主从两个接触面的热流密度分别为

$$q_m = q_k + q_r + f_m q_g, \tag{1}$$

$$q_s = -q_k - q_r + f_s q_g, \tag{2}$$

式中：q_k 为热传导产生的热流密度；q_r 为热辐射产生的热流密度；q_g 为表面单元摩擦产生的热流密度；f_m 和 f_s 为影响流入每个接触面的热流密度大小的参数。

采用 Coulomb 摩擦定律来进行定义搅拌摩擦焊接过程中的搅拌头与焊接构件的接触特征。在焊接过程中滑动摩擦应力 τ 由接触面摩擦系数 μ 和接触压力 p_c 决定，即

$$\tau = \mu \cdot p_c。 \tag{3}$$

1.3 计算成本评估

基于逐个单元的估算，稳定极限 Δt^m_{stable} 可由下式定义，即

$$\Delta t^m_{stable} = \frac{L_{min}}{c_d}, \tag{4}$$

式中：L_{min} 为最小单元的长度；c_d 为材料波速，受材料性质影响，即

$$c_d = \sqrt{\frac{\lambda + 2\mu}{\rho}}, \tag{5}$$

式中：λ，μ 为 Lame 常数；ρ 为密度。

从波速的定义可以看出波速是与材料密度有关的，当把材料密度放大时，稳定极限将增大，此时只需要比较少的增量步，可以大量节省计算时间，但是动能与内能的比率要求不超过 10%[9]。

2 计算结果和讨论

图 3 所示为搅拌头周围焊接构件上表面后退侧材料的流动情况，当搅拌头开始平移时，在轴肩边界的旋转和挤压作用下，质点被旋推到搅拌头的后方，所跟踪的质点并没有进入轴肩下面的区域，这主要是由于上表面的材料受到轴肩边缘的限制，导致材料不能从焊具前方进入轴肩下面的区域。(说明：关于材料流动的视图选取并不一致，导致同样是前进侧后退侧，视觉效果不同，请读者阅读时注意结合文字说明。)

通过以上分析，不难发现，在搅拌摩擦焊接过程中，焊接构件上表面的材料是在轴肩边缘的旋推作用下发生运动的，这是导致搅拌摩擦焊接中出现飞

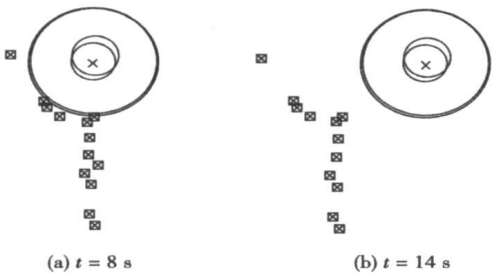

图 3　后退侧上表面材料的流动情况

Fig. 3　Material flow on top surface at retreating side

边现象的主要原因。

图 4 所示为搅拌头周围位于前进侧的上表面材料的流动情况。和图 3 的对比发现，前进侧材料发生绕搅拌头的旋转，而后退侧材料不会发生绕搅拌头的旋转，搅拌摩擦焊接中这一材料流动的规律已经被众多工作所证实[8-10]。

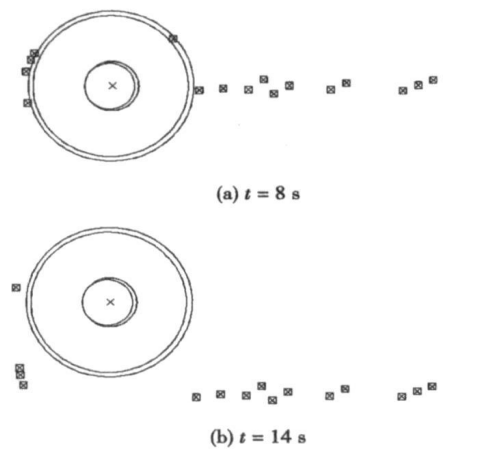

图 4　前进侧上表面材料的流动情况

Fig. 4　Material flow on top surface at advancing side

图 5 所示为后退侧焊接构件中间部分的材料流动情况，从图中可以看出，焊接过程中后退侧材料进入了轴肩下方的区域，在搅拌头的旋转作用下，被旋推到搅拌头的后方。后退侧焊接构件中间部分的材料没有发生绕搅拌头的旋转，而是直接被搅拌头旋推到后方尾迹中。

图 6 所示为前进侧焊接构件中间部分的材料流动情况。和图 5 比较发现，前进侧的材料发生较为明显的搅拌头旋转。值得注意的是，物质点开始接触搅拌头之后，随着搅拌摩擦焊接过程的继续进行，与搅拌针接触的物质点开始脱离焊接构件——搅拌针接触面，开始向外运动，并逐渐运动到轴肩的边缘，由于轴肩的形式是一个锥形，因此，在材料物质点脱离接触面向外运动的过程中，材料具有向下运动的趋势。

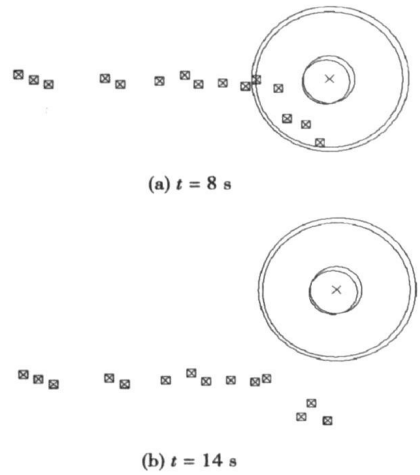

图 5　后退侧焊接构件中间部分的材料流动情况

Fig. 5　Material flow near middle of the welding plates at retreating side

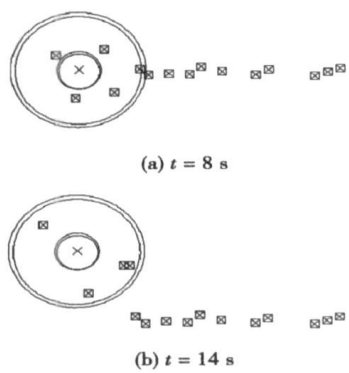

图 6　前进侧焊接构件中间部分的材料流动情况

Fig. 6　Material flow near middle of welding plates at advancing side

图 7 所示为后退侧焊接构件下表面材料流动情况，对比发现，焊接构件中部和底部后退侧材料的流动具有较为明显的区别，在 $t=8$ s 时，焊接构件中部的材料已经开始被搅拌头旋推向搅拌头的后方，然而，在焊接构件底部的材料还没有被搅拌头旋推向搅拌头后方，这说明相对于焊接构件底部而言，在焊接构件中部搅拌头周围材料的流动层较厚，从而导致焊接构件中部的材料物质点具有更强的流动性。

图 8 所示为前进侧焊接构件下表面材料流动情况，在 $t=8$ s 时刻物质点发生了绕搅拌头的旋转，并持续了数周，和图 6 的对比发现，所跟踪的物质点

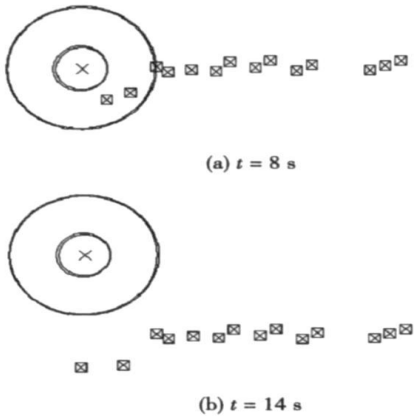

图 7 后退侧焊接构件下表面材料流动情况

Fig. 7 Material flow on bottom of welding plates at retreating side

在绕搅拌针进行旋转时，没有随焊接过程的进行发生沿搅拌头径向方向的明显移动，这说明以搅拌头为参考系，在搅拌头轴肩下面的区域中，材料物质点产生径向的运动的主要原因在于搅拌头轴肩的影响，在焊接构件底部，轴肩的影响很小，此时，搅拌针周围物质点的运动几乎不受轴肩的明显作用，导致计算结果非常接近二维材料流动的情况[8]，这同时也说明二维搅拌摩擦焊接模拟对应的是搅拌摩擦焊接构件底部材料的运动情况。

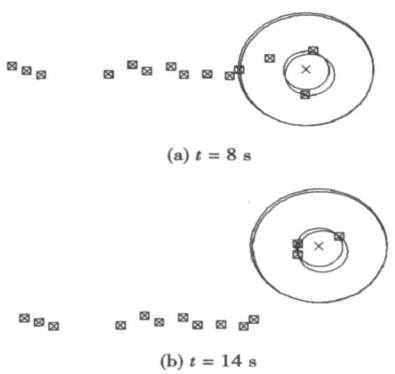

图 8 前进侧焊接构件下表面材料流动情况

Fig. 8 Material flow on bottom of welding plates at advancing side

图 9 所示为搅拌摩擦焊接构件上的温度场分布情况，搅拌摩擦焊接中温度的最大值达到了 445 ℃，在相同的焊接过程参数情况下，试验测得的 Al6061—T_6 合金搅拌摩擦焊接过程的最高温度为 445 ℃[11]，数值结果和试验结果非常接近，也证明了模型的有效性和正确性。从图 9b 可以看出，焊接过程中的温度场在 t=4 s 之后就进入了稳定状态，尽管还有小的波动，但是总体而言，焊接温度已经比较稳定。

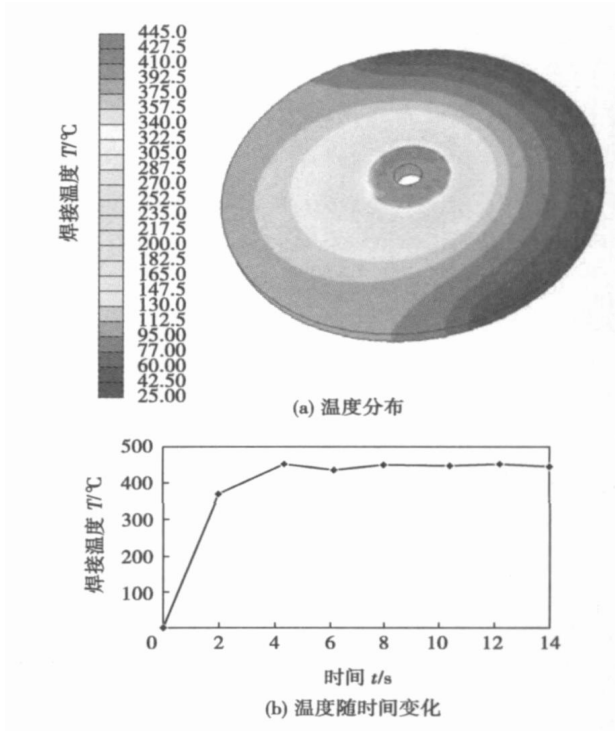

图 9 搅拌摩擦焊接中的温度分布

Fig. 9 Temperature distribution in friction stir welding

图 10 所示为搅拌摩擦焊接构件的等效塑性应变分布情况，从焊接构件的纵向截面可以看到，搅拌摩擦焊接构件的等效塑性应变上表面较大，下表面较小，这主要是由于焊接构件上表面的材料受到搅

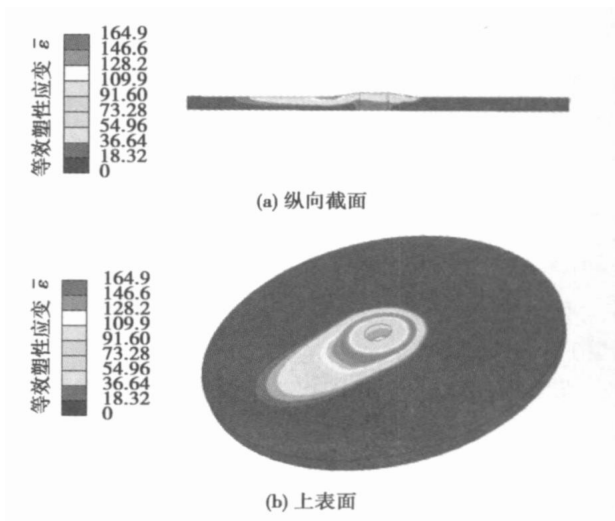

图 10 搅拌摩擦焊接构件等效塑性应变分布

Fig. 10 Distribution of equivalent plastic strain in friction stir weld

拌头轴肩的作用非常明显，而在焊接构件下表面，材料变形主要取决于搅拌针的运动，轴肩的影响迅速减小导致焊接构件下表面材料变形小于上表面。另外，从图 10b 也可以发现，焊接构件上表面的等效塑性应变的最大值产生在搅拌头轴肩的边缘，这和材料的流动行为是相联系的。从前面的分析可知，上表面的材料受到轴肩边缘的作用而未能进入搅拌头轴肩下面的区域，而是直接被轴肩的边缘旋推到搅拌头的后方，因此，上表面等效塑性应变的最大值产生在轴肩的边缘。

3　结　　论

（1）在搅拌摩擦焊接过程中，焊接构件上表面的材料是在轴肩边缘的旋推作用下发生运动的，这是导致搅拌摩擦焊接中出现飞边现象形成的主要原因。

（2）搅拌摩擦焊接构件在不同厚度上材料的流动形式是不相同的，靠近上表面的材料明显受到轴肩运动的影响，而轴肩的运动很难对下表面材料的运动产生大的影响，并且靠近下表面的材料运动非常接近于二维情况。

致　谢：感谢中国科学院金属研究所马宗义研究员和哈尔滨工业大学材料科学与工程学院刘会杰教授与作者的有意义的探讨和给予作者的帮助。

参考文献：

[1]　王大勇，冯吉才，王攀峰. 搅拌摩擦焊接 Al－Li 合金接头的微观组织及力学性能[J]. 金属学报，2004，40：504－508.

[2]　Liu H J，Chen Y C，Feng J C. Effect of zigzag line on the mechanical properties of friction stir welded joints of an Al-Cu alloy[J]. Scripta Materilia，2006，55：231－234.

[3]　Feng J C，Chen Y C，Liu H J. Effects of post-weld heat treatment on microstructure and mechanical properties of friction stir welded joints of 2219－O aluminium alloy[J]. Materials Science and Technology，2006，22(1)：86－90.

[4]　Reynolds A P，Tang W，Khandkar Z，*et al*. Relationships between weld parameters，hardness distribution and temperature history in alloy 7050 friction stir welds[J]. Science and Technology of Welding and Joining，2005，10(2)：190－199.

[5]　Mishra R S，Mahoney M W，McFadden S X，*et al*. High strain rate superplasticity in a friction stir processed 7075 Al alloy[J]. Scripta Materilia，1999，42(2)：163－168.

[6]　Ma Z Y，Sharma S R，Mishra R S. Effect of friction stir processing on the microstructure of cast A356 aluminum[J]. Materials Science and Engineering A，2006，433：269－278.

[7]　Zhang H W，Zhang Z，Chen J T. 3D modeling of material flow in friction stir welding under different process parameters[J]. Journal of Materials Processing Technology，2007，183：62－70.

[8]　张洪武，张　昭，陈金涛. 搅拌摩擦焊接过程的有限元模拟[J]. 焊接学报，2005，26(9)：13－18.

[9]　Hibbit，Karlsson，Sorensen. ABAQUS analysis user manual[M]. USA：Hibbit，Karlsson and Sorensen Incorporation，2003.

[10]　Guerra M，Schmidt C，McClure J C，*et al*. Flow patterns during friction stir welding[J]. Materials Characterization，2003，49：95－101.

[11]　Mcclure J C，Feng Z，Tang W，*et al*. A thermal model of friction stir welding[C] //Proceedings of the 5th International Conference on Trends in Welding Research. Pine Mountain：ASM International，1998.

作者简介：张　昭，男，1979 年出生，博士，讲师。研究方向为制造工艺力学。发表论文 30 余篇。

Email：zhangz@dlut.edu.cn

MAIN TOPICS, ABSTRACTS & KEY WORDS

TIG arc constricted by rotating ceramic plates ZHU Liang, ZHANG Renjun, TIAN Yuji (State Key Laboratory of Gansu Advanced Non-ferrous Metal Materials, Lanzhou University of Technology, Lanzhou 730050, China). p1—4

Abstract: Arc constriction is an effective approach to enhance the heat intensity of TIG (tungsten inert-gas) arc. A novel approach to constrict the TIG arc was presented. By means of double ceramic plates with parallel rotation, the arc near the electrode was constricted. Through observation of the arc shapes and measurement of the welds cross-sections, the arc shapes and its heat characteristics have been investigated at a variety of constriction conditions given by the rotating ceramic plates. The results show that the axially asymmetrical constriction of TIG arc was made by rotating ceramic plates. In the direction perpendicular to the rotating plane of ceramic plates, the central current carried column of the arc was constricted stably. Decrease of the distance between two ceramic plates, and increase of the depth for the arc entering into the ceramic plate gap gave rise to the further constriction of the central current carried column of the arc, and in turn increase the penetration of welds. Furthermore, the arc voltage was increase slightly when the constriction extent became stronger.

Key words: constricted arc; rotating ceramic plates; arc profile

3D modeling of task space for tele-robotic welding based on stereo vision GAO Hongming, LIANG Zhimin, DONG Na, WU Lin (State Key Laboratory of Advanced Welding Production Technology, Harbin Institute of Technology, Harbin 150001, China). p5—8

Abstract: In order to overcome the disadvantage of the human tele-operation, there is need to improve the intelligence level of the tele-robotic welding system. Accurate 3D modeling of the task space is the essential foundation for telerobotic planning, motion control and other automatic function. Stereo vision is employed for task space analysis and 3D reconstruction of telerobotic welding. Stereo matching is accomplished by man-machine interaction combined with subpixel corner feature detection algorithm, in which the Harris corner is first detected then the subpixel refine is made. So that the complicated calculation and low robustness of the automatic visual modeling algorithm is avoided. The experimental 3D reconstruction results of task space have shown the validity of the technique.

Key words: stereo vision; telerobotic welding; 3D reconstruction; task space

Influence of heat treatment on interfacial diffusion of Al alloy cold spraying coating on magnesium alloy YUAN Xiaoguang, LIU Yanxue, WANG Yisong, HUANG Hongjun (School of Material Science and Engineering, Shenyang University of Technology, Shenyang 110023, China). p9—12, 16

Abstract: The Al-12Si-3Fe-3Mn-2Ni alloy powder has been sprayed on the surface of magnesium alloy with cold spraying technology. The interface morphology between substrate alloy and coating has been investigated. The effect of heat treatment temperature and holding time on the diffusion behavior between coating and substrate alloy has been studied. The results show that the Al-12Si-3Fe-3Mn-2Ni alloy powder coating by cold spraying technology becomes more density and homogeneous after heat treatment. Al in the coating diffuses into the substrate alloy and Mg in the substrate alloy diffuses into the coating. Moreover, the diffusion amount diffused into the coating from the substrate alloy is more than that diffused into the substrate alloy from the coating. With an increase of temperature and holding time, the diffusion degree of Al and Mg between the coating and substrate alloy get sufficient. However, the diffusion layer varies little when the temperature rises to 300 ℃ and the holding time increases to 3 h. Little diffusion of other alloying elements in the coating and substrate alloy has been observed.

Key words: magnesium alloy; cold spraying; aluminum alloy powder; diffusion

Effects of Ti—Si on properties of plasma arc "in-situ" welding for SiC_p/Al MMCs CHEN Xizhang, LEI Yucheng, LI Xian, ZHANG Jianhui (School of Material Science and Engineering, Jiangsu University, Zhenjiang 212013, Jiangsu, China). p13—16

Abstract: In order to analyze weldability of SiC particle reinforced aluminum metal matrix composites (SiC_p/Al MMCs), plasma arc "in-situ" welding of SiC_p/Al MMCs are carried out using argon-nitrogen mixture as plasma gases and Ti—Si mixed powder as "in-situ" welded material. The results show that the dense metallurgical joining with obscure interface could be acquired by adding Ti-Si mixed powder into the pool and new composite reinforced are produced in the weld, and the needle-like phases are not found yet, ensuring the quality of joints. The mechanical testing results show that the maximum tensile strength obtained with Ti-Si mixed powder as "in-situ" material are 232.3 MPa. Furthermore the forming mechanism of porosity in welded joint and the corresponding measures are discussed.

Key words: SiC_p/Al metal matrix composites; plasma arc; in-situ welding; Ti-Si

Material flow patterns in friction stir welding ZHANG Zhao, LIU Yali, CHEN Jintao, ZHANG Hongwu (State Key Laboratory of Structural Analysis for Industrial Equipment, Dalian University of Technology, Dalian 116024, Liaoning, China). p17—21

Abstract: Friction stir welding process is simulated by using a fully coupled thermo-mechanical model. The material flow patterns in the friction stir welding process are analyzed. The comparison with

experimental results can validate the current model and shows that the material flows and temperature distributions can be predicted precisely. From the research on material flows around the welding tool, the formation of weld fash in friction stir welding is explained. The 3D material flow patterns on different thicknesses are studied, which is compared with the 2D case to show that the material flows obtained in 2D numerical simulation correspond to the ones near the bottom surface obtained in 3D simulation. The equivalent plastic strain distribution also shows that the shoulder can affect the material behaviors near the top surface and the effect of the shoulder becomes weaker near the bottom surface, which demonstrates that the 2D case correspond to the part near the bottom surface in 3D case.

Key words: friction stir welding; fully coupled thermo-mechanical model; material flow patterns; finite element method

Electrode arc equation and thermodynamic analysis of submerged arc welding with constant current power supply LIU Chaoying[1], HUANG Shisheng[2] (1. Faculty of Electronic Information and Mechatronic Engineering, Zhaoqing University, Zhaoqing 526061, Guangdong, China; 2. Faculty of Mechanic Engineering, South China University of Technology, Guangzhou 510640, China). p22—24

Abstract: The submerged arc welding (SAW) system consists of an inverted welding power supply with constant current output character, a wire feeder, a welding traveller and a controller. Taking the arc voltage and the setting voltage as input parameters, the controller gives a DC output, which is modulated in pulse width modulation scheme, to drive and adjust the wire feeding speed. A mathematical model related to the welding arc and the wire feeding speed during SAW is established in the form of a first order equation. The model described the balance relation between burning the procedure of the wire in the arc and the feeding of the wire via the wire-feeder. According to thermodynamic analysis of the power supply, molten pool and wire, a scheme for the selection of the wire diameter is obtained, on basis of the diameter of the wire being in proportion to the square root of the welding current. A detailed equation between the wire diameter and the welding current is reported.

Key words: submerged arc welding; dynamic model; thermodynamic analysis; wire diameter

Optimal path modeling for redundant robot based on genetic algorithm LIU Yong[1], Wang Kehong[1], Yang Jingyu[2] (1. Department of Material Science and Engineer, Nanjing University of Science and Technology, Nanjing 210094, China; 2. School of Coputer Science and Fechnology, Nanjing University of Science and Technology, Nanjing 210094, China). p25—28

Abstracts: To solve the optimizing problem of the path planning of robot with eleven degree-of-freedom, a multi-object mathematical model and solution plan has been proposed and analyzed. Using genetic algorithm as optimizing method, a adapive degree function was built. The suitable parameter was obtained through lots of practices. The genetic algorithm procedure was designed and realized. Based on this algorithm, optimizing experiments were carried out based on typical space transversal weld by using under 3 degree-of-freedom gantry and 6 degree-of-freedom robot. Results of experiments indicate that the suitable solution can be quickly found through the algorithm. This algorithm was simulated and also loaded to robot controller to do welding experiments. And the results show that robot joints move steady under the best position of robot placement and good welds have been acquired. It shows this method is correct and feasible.

Key words: redundant welding robot; path planning; genetic algorithm

Heating effect of plasma jet and particle flux in plasma spray XIA Weisheng[1], ZHANG Haiou[2], WANG Guilan[1], YANG Yunzhen[1], ZOU Yang[1] (1. State Key Laboratory of Material Processing and Die & Mould Technology, Huazhong University of Science & Technology, Wuhan 430074, China; 2. State Key Laboratory of Digital Manufacturing and Equipment Technology, Huazhong University of Science & Technology, Wuhan 430074, China). p29—32

Abstract: The length of plasma jet was obtained on the basis of digital image processing and the CCD image gathering system, and heating effect was determined through the temperature rising of a substrate in the unit time by an IR pyrometer. Then comparative experiments of heating effect by plasma jet and particle flux were carried out under different spray distances and lengths of plasma jet to analyze their characteristics. Experimental results show that when the length of plasma jet is shorter than or equal to the spray distance, heating effect is dominated by plasma jet. However, if the length is longer than the spray distance, the heating effect of particle flux becomes more and more obvious, but the case for plasma jet drops rapidly. Therefore, the length of plasma jet, as a characteristic evaluation index, can be adopted to select the reasonable spray distance. This is certified by the patterns and cross-section thickness profiles of deposited coatings under different spray distances.

Key words: plasma spraying; heating effect; plasma jet; particle flux; plasma jet length; spray distance

Fe-based alloy composite coating reinforced by Ti($C_{0.3}N_{0.7}$) particle through laser cladding technology QI Yongtian, ZOU Zengda, QU Shiyao, ZHU Qingjun (School of Materials Science and Engineering, Shandong University, Jinan 250061, China). p33—36

Abstract: A new in-situ synthesis method is carried out to produce Fe-based alloy composite coating reinforced by Ti($C_{0.3}N_{0.7}$) particle on the Q235 mild steel through CO_2 laser cladding technology. X-ray diffraction is used for phase identification in the composite coating. The microstructure of laser cladding layer is analyzed by means of optical microscopy, scanning electron microscopy, and electron probe microscopy analyzer. The microhardness distribution is measured by using microhardness tester. The results show that Ti($C_{0.3}N_{0.7}$) particle is produced by an in-situ metallurgical reaction of TiN particle and graphite powder during laser cladding process. The shape of some Ti($C_{0.3}N_{0.7}$) particle is similar to rhombus, and the others are irregular shape. Size of the fine Ti($C_{0.3}N_{0.7}$) particles is within 0.1—5 μm, and evenly in dispersed the matrix. The micro-